ADVANCED FUNCTIONAL MATERIALS
www.afm-journal.de

Dual-Mode Film Based on Highly Scattering Nanofibers and Upcycled Chips-Bags for Year-Round Thermal Management

*Qimeng Song, Stefan Rettinger, Chengzhang Xu, Ulrich Mansfeld, and Markus Retsch**

Advanced thermal management is crucial in mitigating the escalating global energy consumption and alleviating associated climatic and environmental issues. Here, a dual-mode film that integrates solar heating and radiative cooling functionalities for year-round thermal management is introduced. The cooling side of the film, composed of PCL-SiO_2 composite nanofibers, exhibits an impressive solar reflection of 0.98 and a mid-infrared emissivity of 0.91, resulting in sub-ambient cooling performance under intensive sunlight. Meanwhile, the heating side of the film, based on the ink side of the upcycled chip bags, efficiently harvests thermal energy from sunlight, leading to a temperature rise of 16.5 °C. The cooling and heating modes of the film can be switched by flipping it. With its outstanding optical properties, weathering durability, and switchable heating and cooling modes, the dual-mode film holds great potential for year-round energy savings with minimal environmental impact due to its sustainable composition and easy fabrication.

1. Introduction

Maintaining optimal indoor temperatures through heating and cooling operations represents a substantial portion, almost 25%, of the energy produced worldwide.[1] This demand, particularly for cooling, is anticipated to continuously escalate, driven by the compounding effects of global warming and the worsening of extreme climatic conditions.[2–4] Despite advancements in renewable energy sources, continued reliance on fossil fuels for thermal management remains a significant contributor to **anthropogenic climate change** associated with greenhouse gas emissions.[5,6] Therefore, implementing **sustainable and energy-efficient strategies** for heating and cooling is crucial to achieving the goal of zero-carbon emissions by 2050. With its ability to achieve cooling without any energy input, the passive daytime cooling technique is considered a promising sustainable strategy to alleviate the energy demand for cooling,[7–9] as well as enhance personal thermal comfort.[10,11] By optimizing the optical properties to minimize absorption in the solar spectrum and maximize thermal radiation within the atmospheric transparency window (8–13 μm), sub-ambient cooling has been successfully demonstrated during daylight hours, even under intense solar irradiation.[12–17] However, while these cooling devices are effective in hot conditions, they also provide cooling in cold conditions when heating is required, resulting in additional energy consumption. This energy expenditure may offset the energy saved during hot periods.

Intelligent radiative cooling devices, which integrate heating and radiative cooling functionalities, have recently garnered significant attention for achieving year-round energy savings.[18–20] By efficiently converting sunlight into heating energy, these smart devices enable heating mode operation in cold conditions characterized by high solar absorption. Conversely, the cooling function is activated by altering the optical properties of the device to exhibit low solar absorption and high thermal emission. The transition between the heating and cooling mode can occur automatically through physical stimuli, such as voltage,[21] and temperature changes,[22–25] or through straightforward manual manipulation, e.g. flipping between different sides of the devices.[26–29] Despite the impressive cooling and heating performance achieved by current dual-mode devices, limited scalability associated with sophisticated fabrication processes has hindered their practical application. Furthermore, using non-environmentally friendly materials, like poly(vinylidene fluoride) (PVDF), exacerbates environmental concerns. To address these challenges, increasing efforts have been directed toward exploring biodegradable polymers, such as polycaprolactone (PCL) and

Q. Song, S. Rettinger
Department of Chemistry
Physical Chemistry I
University of Bayreuth
Universitätsstraße 30, 95447 Bayreuth, Germany
C. Xu
Department of Chemistry
Macromolecular Chemistry II
University of Bayreuth
Universitätsstraße 30, 95447 Bayreuth, Germany
U. Mansfeld
Bavarian Polymer Institute
University of Bayreuth
Universitätsstraße 30, 95447 Bayreuth, Germany
M. Retsch
Department of Chemistry
Physical Chemistry I
Bavarian Polymer Institute
Bayreuth Center for Colloids and Interfaces
and Bavarian Center for Battery Technology (BayBatt)
University of Bayreuth
Universitätsstraße 30, 95447 Bayreuth, Germany
E-mail: markus.retsch@uni-bayreuth.de
The ORCID identification number(s) for the author(s) of this article can be found under https://doi.org/10.1002/adfm.202425458

DOI: 10.1002/adfm.202425458

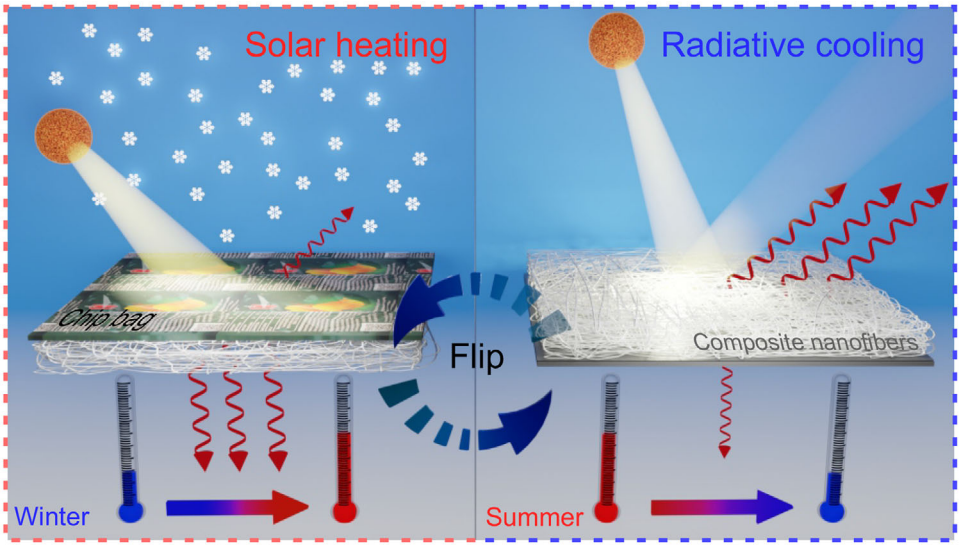

Figure 1. Schematic diagram of dual-mode film for year-round heating and cooling.

polylactic acid (PLA), as potential alternatives for scalable and eco-friendly dual-mode radiative cooling solutions.[30–32] Additionally, the sustainability of membrane-based technologies is gaining increasing attention, particularly regarding the recyclability and biodegradability of polymeric membranes.[33,34]

In this work, a sustainable and scalable dual-mode film for year-round thermal management was composed by integrating a nanofibrous nonwoven onto upcycled chip bags. The cooling side, with exceptional solar scattering (0.98) and high mid-infrared (MIR) emission (0.91), was achieved by PCL-SiO_2 composite nanofibers fabricated using the solution blow spinning (SBS) technique. This side provides daytime sub-ambient cooling under intense sunlight. As for the heating side, the chip bags' ink side exhibits high solar absorption and relatively low thermal emission, effectively converting the sunlight into thermal energy. Positioning the appropriate side of the dual-mode film facing the sky enables either solar heating or radiative cooling to meet specific climatic conditions, achieving year-round energy savings.

2. Results

Figure 1 illustrates the schematic diagram of the dual-mode film for all year-round solar heating and radiative cooling. The dual-mode film consists of a PCL-SiO_2 composite nanofiber nonwovens supported on reused chip bags. SiO_2 nanoparticles are blended into the nanofibers to enhance the film's emissivity within the atmospheric transparency window regime. In hot weather, the cooling functionality of the dual-mode film is activated by positioning the PCL-SiO_2 nanofiber nonwoven facing the sky. The nanofiber nonwoven, with a fiber diameter comparable to the solar wavelengths (250–2500 nm), possesses a strong scattering of sunlight, thereby minimizing energy absorption from the sunlight. Simultaneously, the high MIR emissivity of the SiO_2-blended PCL nanofibers facilitates efficient heat transfer from the film to the cold outer space (≈3K) via thermal radiation, consequently achieving sub-ambient cooling during daytime.

Conversely, in cold weather, when heating is desired, the chip bags' ink side is orientated toward the sky. This side of the chip bags, characterized by strong solar absorption, enables the thermalization of sunlight, thereby mitigating the energy demand for heating purposes. Year-round energy savings are thus attainable through solar heating and radiative cooling by simply flipping the dual-mode film.

PCL, a cost-efficient and readily available biodegradable polymer, has found extensive use in biomedical applications, such as tissue engineering and drug delivery.[35,36] Its biodegradability through microbial action has been extensively demonstrated in state-of-the-art studies.[37,38] Additionally, sustainable routes for PCL synthesis have also been explored, reducing its environmental impact across the entire lifecycle.[39] In this work, PCL nanofibers were fabricated using the SBS technique, as illustrated schematically in **Figure 2a**. Compared to the widely utilized fiber fabrication technique, electrospinning, which demands sophisticated setups and high-voltage power, SBS is characterized by its simplicity and ease of operation.[40,41] Although SBS presents challenges in controlling fiber uniformity compared to electrospinning, the resulting nanofibers with a broad range of diameters are advantageous for broadband solar reflection, as they enhance solar scattering across a wide wavelength range. In addition, the fiber production rate of SBS is similar to or even higher than electrospinning,[42] and holds great promise for further optimization making it a potentially scalable technique for large-area nanofiber fabrication and practical applications.[43] With the pressurized gas carrying the PCL solution through the nozzle (diameter of 0.3 mm), the PCL nanofibers were formed using a commercial airbrush. These nanofibers were then collected with a roller collector coated with a supporting foil, such as an aluminum (Al) foil or a chip bag. The fiber production rate of the current SBS setup (single nozzle) used in this work is ≈1.5 g h^{-1}. The photograph in Figure 2b shows the resulting PCL nanofibers nonwoven collected on an Al foil. The white color of the nonwoven indicates its strong solar scattering performance, attributed to the multilayer structure of randomly stacked

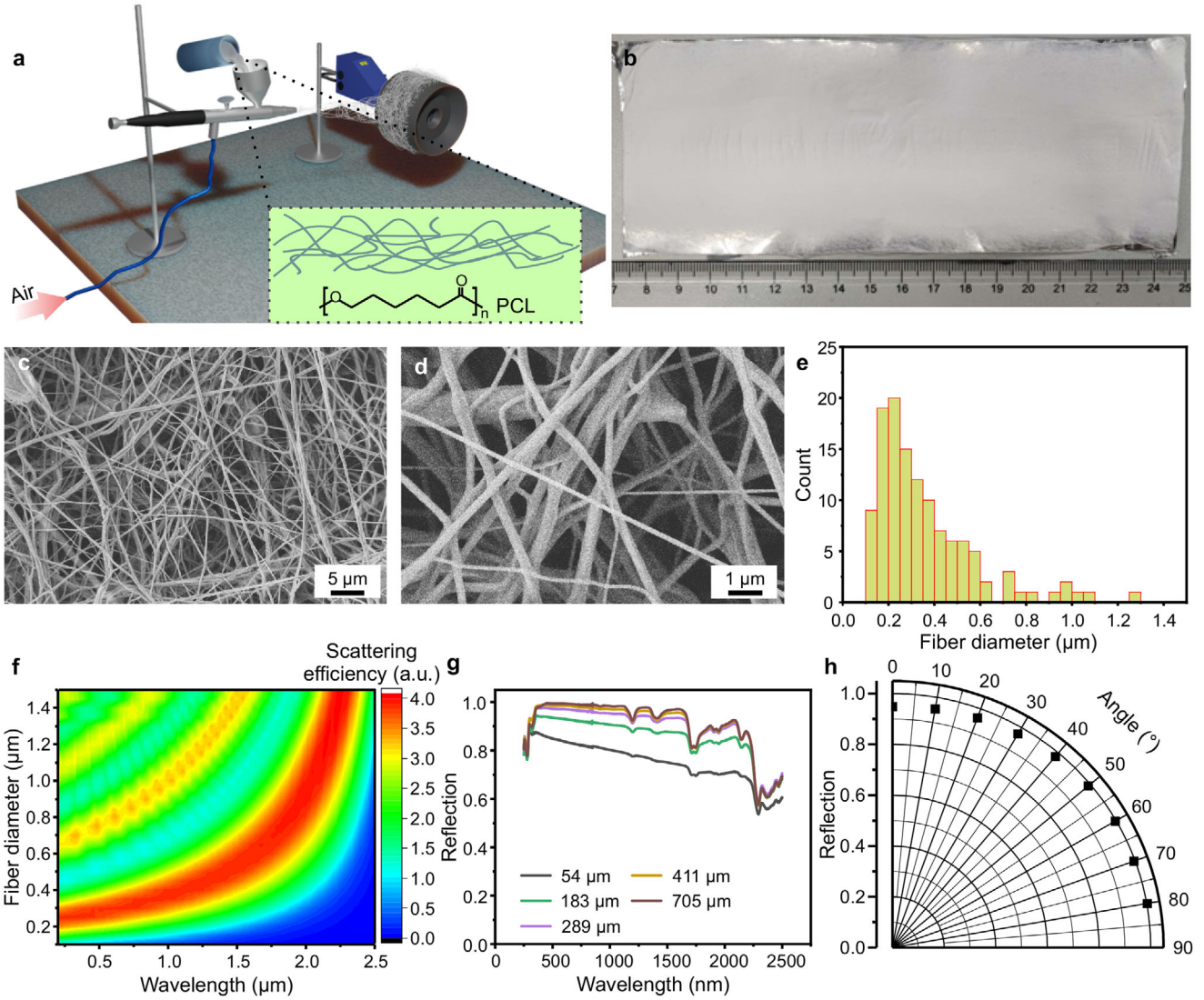

Figure 2. a) Schematic of the fabrication of PCL nanofibers via solution blow spinning with an airbrush. b) Photography of a PCL fibers nonwoven. c) and d) SEM images of PCL nanofibers with different magnifications. e) Distribution of PCL fiber diameters. f) FDTD simulation of the spectral scattering efficiency of individual PCL nanofibers as a function of their fiber diameter. g) UV/Vis spectrum of PCL nanofibers nonwoven with various thicknesses. h) Average solar reflection of PCL nanofibers nonwoven at different incidence angles.

nanofibers with polydisperse diameters. In contrast, the compact PCL film is highly transparent (Figure S1, Supporting Information). The morphology and diameter of the PCL nanofibers were analyzed using a scanning electron microscope (SEM), as depicted in Figure 2c,d. The size distribution of the nanofibers' diameter is presented in Figure 2e, showing a range of fiber diameter from 0.1 to 1.3 μm. This broad distribution, comparable to the solar wavelength, ensures a strong scattering of broad-band sunlight, consistent with Finite-Difference Time-Domain (FDTD) simulation results based on Mie theory (Figure 2f; Figure S2, Supporting Information). Furthermore, the impact of the nonwoven thickness on its solar reflectivity was also investigated. Nanofiber nonwovens of various film thicknesses were obtained by adjusting the spinning time. It was observed that an increase in nonwoven thickness enhances the solar reflection of the nanofiber until a plateau is reached (Figure 2g). A maximum solar reflection is achieved with a nonwoven thickness of ≈400 μm, demonstrating an exceptional angular-dependent average reflection of up to 0.96 in the solar range (Figure 2h; Figures S3, S4, Supporting Information). The average solar reflection was calculated based on the spectrum of AM 1.5 solar irradiation,[44] with detailed information in the Supplementary Information (SI).

PCL nanofibers exhibit remarkable solar scattering capabilities, significantly reducing light absorption from sunlight. To emphasize this characteristic further, a graphite-coated Al foil was coated with PCL nanofibers. The average solar reflection of the graphite-coated Al foil increased significantly from 0.11 to 0.95 upon covering by PCL nanofibers (Figure S5, Supporting Information), demonstrating a substantial reduction in solar absorption when facing the sun. In addition to high solar scattering, the PCL nanofiber nonwoven possesses a relatively high MIR emissivity in the atmospheric transparency window range,

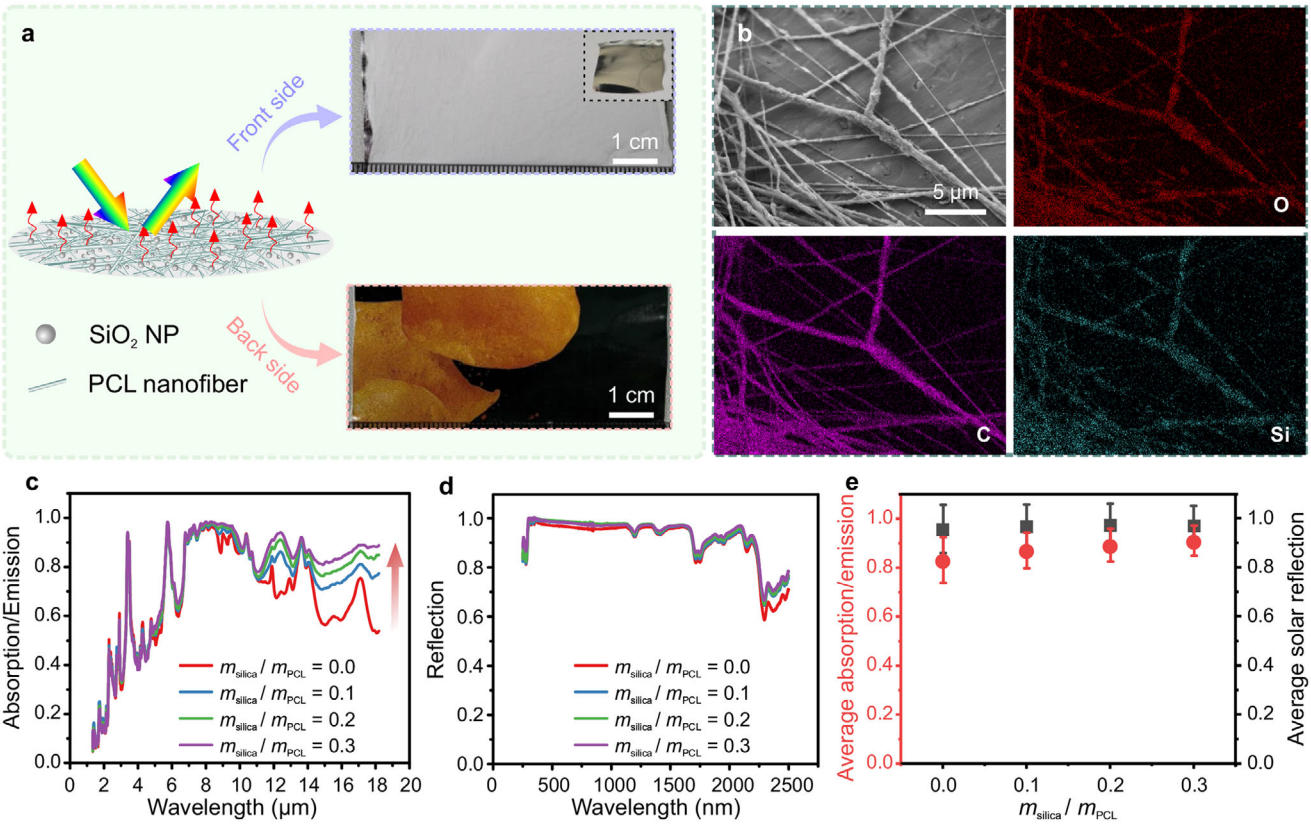

Figure 3. a) Schematic and photography of the SiO_2 nanoparticles embedded in PCL nanofibers on a chip bag. Top: PCL nanofibers side (inset displays the uncoated inside surface of a chip bag); Bottom, chip bag ink side. b) SEM image of PCL-SiO_2 nanofibers and corresponding elemental mapping images of O, C, and Si. MIR absorption (c) and UV/Vis reflection (d) spectrum of PCL nanofibers nonwoven with various contents of SiO_2 nanoparticle. e) Average MIR absorption/emission and solar reflection of PCL nanofibers nonwoven with various SiO_2 nanoparticles contents.

≈0.83 (Figure S6, Supporting Information). To further enhance the emissivity of the PCL nanofiber and to improve its heat dissipation efficiency, SiO_2 nanoparticles were blended into the fibers by mixing them with the PCL precursor solution. **Figure 3a, top** shows the composite nanofibers collected on a reused chip bag (Al side), and Figure 3a, **bottom** illustrates the backside of the chip bag (ink side). SEM images obtained using secondary electron and backscattered electron detection (Figure S7, Supporting Information) and EDX elemental mapping images (Figure 3b) confirm the homogeneous blending of SiO_2 nanoparticles into the PCL fibers.

Furthermore, all fibers with varying SiO_2 nanoparticle contents exhibit a similar hydrophobic surface, with a contact angle of ≈135° (Figure S8, Supporting Information). The consistent contact angle of PCL and PCL-SiO2 implies that the nanoparticles did not change the interfacial properties of the PCL nonwoven. The presence of SiO_2 nanoparticles effectively enhances the MIR emission of the PCL nanofiber nonwoven (Figure 3c). The average absorption/emission in the atmospheric transparency window range increases from 0.83 for unblended PCL nanofibers to 0.91 for PCL-SiO_2 fibers with a m_{PCL}/m_{SiO2} = 0.3 (Figure 3e). Additionally, the inclusion of SiO_2 nanoparticles also slightly enhances the solar light reflection of the nanofiber nonwoven, from 0.96 (PCL) to 0.98 (PCL-SiO_2 fibers with a m_{PCL}/m_{SiO2} = 0.3) (Figure 3d). This enhancement is likely attributed to the structuring on multiple length scales of the PCL-SiO_2 nanofibers.[45,46]

PCL-SiO_2 composite nanofibers exhibit outstanding optical properties in both solar and MIR regimes (**Figure 4a**), with an average solar reflection of up to 0.98 and an average emission of 0.91. To verify the passive cooling performance of the composite nanofibers, its net cooling power was theoretically calculated based on the measured absorption spectra and a widely used radiative cooling theoretical model,[8] with various nonradiative heat transfer coefficients (h_c), i.e., 0, 5, 10, and 15 W/(m^2K). During nighttime, the composites radiate the heat to outer space, providing a net cooling power of 148.4 W m^{-2} (Figure 4b). With minimal solar energy uptake during daytime, a cooling capacity of 125.9 W m^{-2} is expected under a solar irradiation of 1000 W m^{-2}. In addition, with the cooling power equal to zero, different subambient temperatures can be achieved, depending on h_c. For instance, with h_c = 5 W/(m^2K), sub-ambient temperature drops of 16.3 and 13.7 °C can be obtained during nighttime and daytime, respectively.

Aluminum-plastic laminate (APL) has been extensively utilized as packaging material, particularly for potato chips, to prolong the product's shelf life. However, its sophisticated multilayer composition, which includes various types of polymers and aluminum, presents challenges for recycling efforts, leading to significant environmental pollution on a global scale.[47,48] The chip

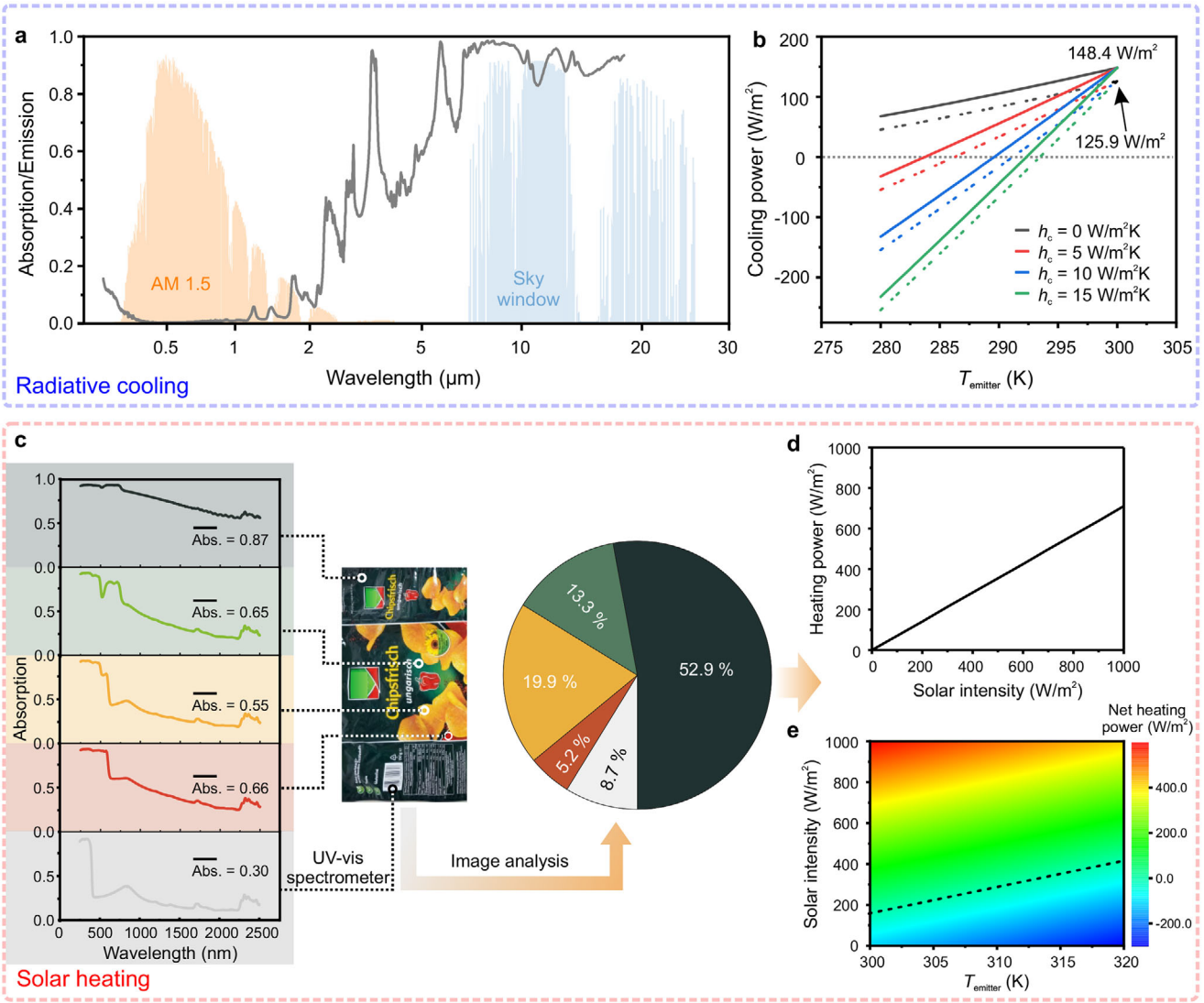

Figure 4. a) Optical properties of a chip bag coated with a PCL-SiO_2 nanofiber nonwoven. The AM 1.5 solar intensity spectrum (highlighted in orange) and atmospheric transparency window (highlighted in blue) were plotted as the background. b) Predicted net cooling power for a chip bag supported PCL-SiO_2 nanofibers nonwoven with various nonradiative heat transfer coefficients (h_c), 0, 5, 10, 15 W/(m^{2}K) for daytime (dashed lines) and nighttime (solid lines). The AM 1.5 solar spectrum with a power intensity of 1000 W m^{-2} was used for daytime calculations. c) Estimation of the average solar absorption of the ink side of the entire chip bag based on the solar absorption spectra of each individual color component. d) Estimated solar heating power as a function of solar radiance intensity. e) Predicted net heating power as a function of solar intensity and emitter temperature, with h_c = 5 W/(m^{2}K). The dashed line indicates zero net heating power. An ambient temperature of 300 K was used for the numerical calculation.

bag possesses two distinct sides: the inner side, characterized by a mirror-like appearance, and the outer side with an ink printing. Due to its high solar reflection capability (up to 0.86), the inner side has already demonstrated its potential as a solar reflector in passive daytime cooling applications.[49,50] Conversely, the outer ink side of the chip bag indicates notable solar absorption (Figure 4c), which varies depending on the ink color, along with low mid-infrared (MIR) emissivity (Figure S9, Supporting Information). This inherent attribute renders it suitable for solar heating applications.

While detecting the solar absorption of the entire chip bag is challenging, a strategy to estimate its average solar absorption by analyzing the spectral reflection of its primary color components is provided here. As shown in Figure 4c, using image analysis, the surface coverage of each color component of an exemplary chip bag was first determined: dark green (52.9%), light green (13.3%), orange (19.9%), red (5.2%), and white (8.7%). Subsequently, the average solar absorption for each color based on their solar reflection spectra was calculated: dark green (0.87), light green (0.65), orange (0.55), red (0.66), and white (0.30). This yielded an average solar absorption of 0.71 for the entire chip bag. Depending on the intensity of solar irradiation, various solar heating performances can be obtained (Figure 4d). For instance, with a solar irradiation intensity of 1000 W m^{-2}, solar heating of ≈710 W m^{-2} is expected. Note that chip bags in the market display diverse patterns, resulting in variations in solar absorption

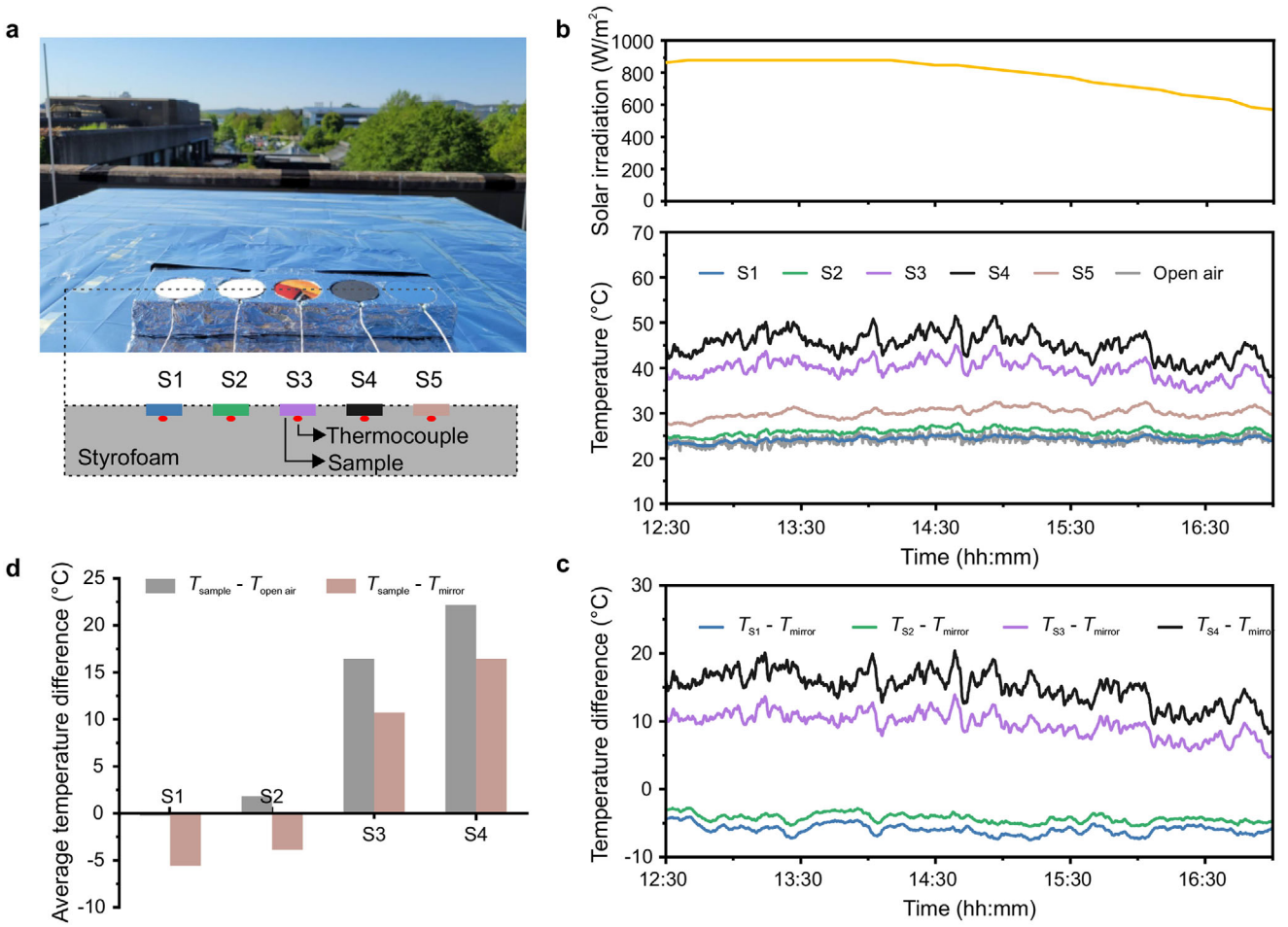

Figure 5. a) Photography and schematic of the homemade setup for field testing. S1: PCL-SiO_2 nanofibers coated chip bag; S2: PCL nanofibers coated graphite-Al foil; S3: ink-side of the chip bag; S4: graphite-Al foil; S5: reference Ag mirror. b) Temperature tracking of the samples and the solar intensity during the field testing. c) The temperature difference between the samples and reference Ag mirror. The measurement was carried out under a clear sky on May 13th, 2024, in Bayreuth, Germany. d) Average temperature difference between samples and open air, and between samples and reference Ag mirror under an average solar intensity of 874 W m^{-2} (12:30-14:30).

(Figure S10, Supporting Information). Selecting a suitably patterned chip bag can likely facilitate different levels of solar heating, catering to global heating demands across different regions and preventing overheating.

When positioned facing the sky, the ink side of the chip bag also emits heat to outer space via thermal radiation, attributed to its non-zero emissivity. Thus, the average emissivity of the entire chip bag in the atmospheric transparency window range was calculated based on the same strategy as estimating the average solar reflectivity (Figure S9, Supporting Information), which amounted to 0.69. The nighttime cooling power of the ink side chip bag with various nonradiative heat transfer coefficients (h_c), i.e., 0, 5, 10, and 15 W/(m^2K), are plotted in Figure S11 (Supporting Information). Based on $P_{\text{net heating}} = P_{\text{solar heating}} - P_{\text{cooling}}$, the net heating power of the entire example chip bag was estimated. The ink side of the chip bag provides various net heating powers depending on its temperature relative to the environment and the solar radiance (Figure 4e; Figure S12, Supporting Information). For instance, a net heating power of ≈600 W m^{-2} can be expected under 1000 W m^{-2} sunlight when the temperature of the chip bag is equal to ambient temperature ($T_{\text{emitter}} = T_{\text{amb}}$).

A dual-mode film, integrating passive cooling and solar heating functionalities, is realized by combining PCL-SiO_2 composite nanofibers with upcycled chip bags. To experimentally demonstrate the heating and cooling abilities of the dual-mode film, continuous field testing was conducted, under a clear sky in Bayreuth, Germany. **Figure** 5a illustrates the photograph and schematic of the setup for field testing. During the measurement, the dual-mode film with different sides facing the sky, PCL-SiO_2 nanofibers (S1), and the chip bag ink-side (S3) were embedded into a styrofoam plate to prevent undesired thermal conduction. The temperature of an Ag mirror (S5), employed as a reference, and the open-air temperature in the shade were also recorded during the test. Besides, the temperatures of graphite-Al foil samples – one coated with a PCL nanofiber film (S2) and one uncoated (S4) – were determined to emphasize the exceptional solar scattering of the PCL nanofibers that have been retrofitted to such strongly absorbing surfaces. Figure 5b shows the recorded temperature of the tested samples over ≈4.5 h (12:30-17:00)

during the daytime under intensive solar irradiation. The temperature difference between the tested samples and the reference Ag mirror is illustrated in Figure 5c. Under direct sunlight with an average intensity of 874 W m^{-2}, the pristine graphite-Al foil (S4) exhibited a temperature increase of up to 19.3 °C higher than the reference Ag mirror temperature due to its high solar absorption (Figure 5d).

In contrast, the graphite-Al foil coated with PCL nanofibers (S2) maintained its temperature lower than the reference Ag mirror. The average temperature difference ($T_{PCL\text{-}graphite\text{-}Al} - T_{mirror}$) is −3.9 °C during the period from 12:30 to 14:30 (Figure 5d). The temperature of the dual-mode film was significantly lower than that of the reference Ag mirror ($T_{PCL\text{-}SiO2} - T_{mirror} = -5.5$ °C) when the cooling side (PCL-SiO_2 nanofibers) faced the sky. In this case, even a sub-ambient temperature relative to the open air ($T_{PCL\text{-}SiO2} - T_{air} = -0.2$ °C) could be observed without protection from convective heat transfer. Upon flipping the film such that the heating side (ink side of the chip bag) faced the sky, the film exhibited a significantly higher temperature, 10.8 °C higher than the reference Ag mirror. The sub-ambient cooling and solar heating achieved by positioning the corresponding sides of the dual-mode film toward the sky confirms its potential for year-round energy savings. In addition, the PCL-SiO_2 nanofiber nonwovens exhibited lower temperatures in comparison to the PCL nanofibers coated graphite-Al foil, indicating the enhanced cooling performance attributed to the presence of SiO_2 nanoparticles and better solar scattering. Whereas the coated graphite-Al foil exhibited a slightly increased solar absorption compared to the coated, reflective chips bags, the MIR emissivity was not increased and merely depended on the optical properties of the PCL nanofibers (Figure S13, Supporting Information). Field testing was also conducted during nighttime, and the temperatures of all samples, as well as the temperature differences between the samples and the reference Ag mirror, are shown in Figure S14 (Supporting Information). In the absence of solar heating, both the PCL-SiO_2 nanofibers nonwoven (S1) and the PCL nanofibers coated graphite-Al foil (S2) exhibited a sub-ambient cooling of ≈3.0 °C, which outperformed the less emissive absorbing side of the chips bag and the broadband emitting graphite-Al foil.

The mechanical properties of the dual-mode film were evaluated through tensile testing. For comparison, the tensile strength of a free-standing PCL-SiO_2 nanofiber nonwoven and a pristine chip bag were also measured. As shown in **Figure 6**a, the free-standing PCL-SiO_2 nanofiber nonwoven exhibits a maximum force of 3.79 N, corresponding to a tensile strength of 9.5 MPa, and an elongation at break of 50.8%, which is comparable to values reported in the literature for electrospun PCL nanofiber nonwovens.[51] The mechanical properties of the dual-mode film, where the PCL-SiO_2 nanofiber nonwoven is supported by the chip bag, are primarily dictated by the chip bag itself. As a result, the dual-mode film demonstrates mechanical performance closely matching that of the chip bag and is significantly stronger than the standalone PCL nanofiber nonwoven. To evaluate the structural integrity of the dual-mode film, a bending test was conducted, as shown in Figure 6b. After 2000 repeated bending cycles, no visible detachment of the nanofiber nonwoven from the chip bag was observed (Figure S16, Supporting Information), confirming strong adhesion and mechanical stability of the composite structure. To further assess the stability of the dual-mode film, it was exposed to outdoor conditions for one month. As illustrated in Figure 6c, the films were fixed to a metal plate positioned at a 30° tilt angle relative to the horizon, with the cooling side (PCL-SiO_2 nanofibers) and the heating side (chip bag) facing the sky. The test period encompassed various weather conditions, such as intense solar radiation, heavy rain, and strong winds. Solar intensity ranged from 0 to over 900 W m^{-2}, while air temperatures varied from 7 to 33 °C. A photograph of the dual-mode film during rainfall is also provided in Figure 6c. The hydrophobicity of the PCL-SiO_2 nanofibers causes the water droplets to roll off the nonwoven surface rather than wetting this porous film. Meteorological data, including solar irradiation, air temperature, wind speed, and relative humidity, were continuously recorded throughout the outdoor test, as shown in Figure S15 (Supporting Information). The broadband optical properties of both the cooling and heating side of the dual-mode film are presented in Figure 6d,e. No obvious changes in solar reflectivity or MIR absorption spectra were observed for either the PCL-SiO_2 nanofibers or the ink side of the chip bag, indicating the excellent outdoor stability of the dual-mode film during this test.

To further demonstrate the year-round energy-saving performance of the dual-mode film, both its cooling and heating capabilities were evaluated using a tailored indoor setup that imitates the field testing for both summer and winter conditions. **Figure 7**a illustrates the schematic of this setup, with detailed information provided in previous work.[52] During the measurement, the "ambient temperature", defined as the temperature of an Ag mirror, was controlled by adjusting the temperature and the volumetric flow rate of the gas flushing between the convection shield and measurement cell. By tuning these parameters, an "ambient temperature" of 3.2 and 32.9 °C was achieved to simulate winter and summer conditions, respectively. In addition, AM 1.5 solar irradiation was provided by a solar simulator, with 100% and 70% of full sun (1000 W m^{-2}) used for the "Summer" and "Winter" measurements, respectively. It should be noted that only 75% of the light reached the samples due to the scattering from the multi-layer convection shield.[51] As a result, the solar intensities incident on the samples were 750 and 525 W m^{-2}, respectively.

The heating side, i.e., ink side of the chip bag, and the cooling side, i.e., PCL-SiO_2 nanofibers, of the dual-mode film were characterized under "Winter" and "Summer" conditions, respectively. For comparison, the temperature of a graphite-Al foil was also measured in both conditions (Figure S17, Supporting Information). As shown in the temperature tracking in Figure 7b,c, the samples were first measured without (w/o) light, and light was then switched on after a steady temperature was reached. In "Winter nighttime", a steady-state temperature of −6.2 °C was recorded for the ink side of the chip bag, which is higher than that of the graphite-Al foil (−8.3 °C) (Figure 7d). This higher temperature is attributed to the reduced thermal emission of the ink side of the chip bag compared to graphite-Al foil, indicating that less energy is required to offset radiative cooling during nighttime. During the daytime, with solar irradiation of 525 W m^{-2}, the temperature of the ink side of the chip bag and graphite-Al foil rose to a similar level, with the ink side of the chip bag at −1.6 °C and the graphite-Al foil at −1.4 °C, demonstrating a comparable heating performance between the two samples. In "Summer nighttime"

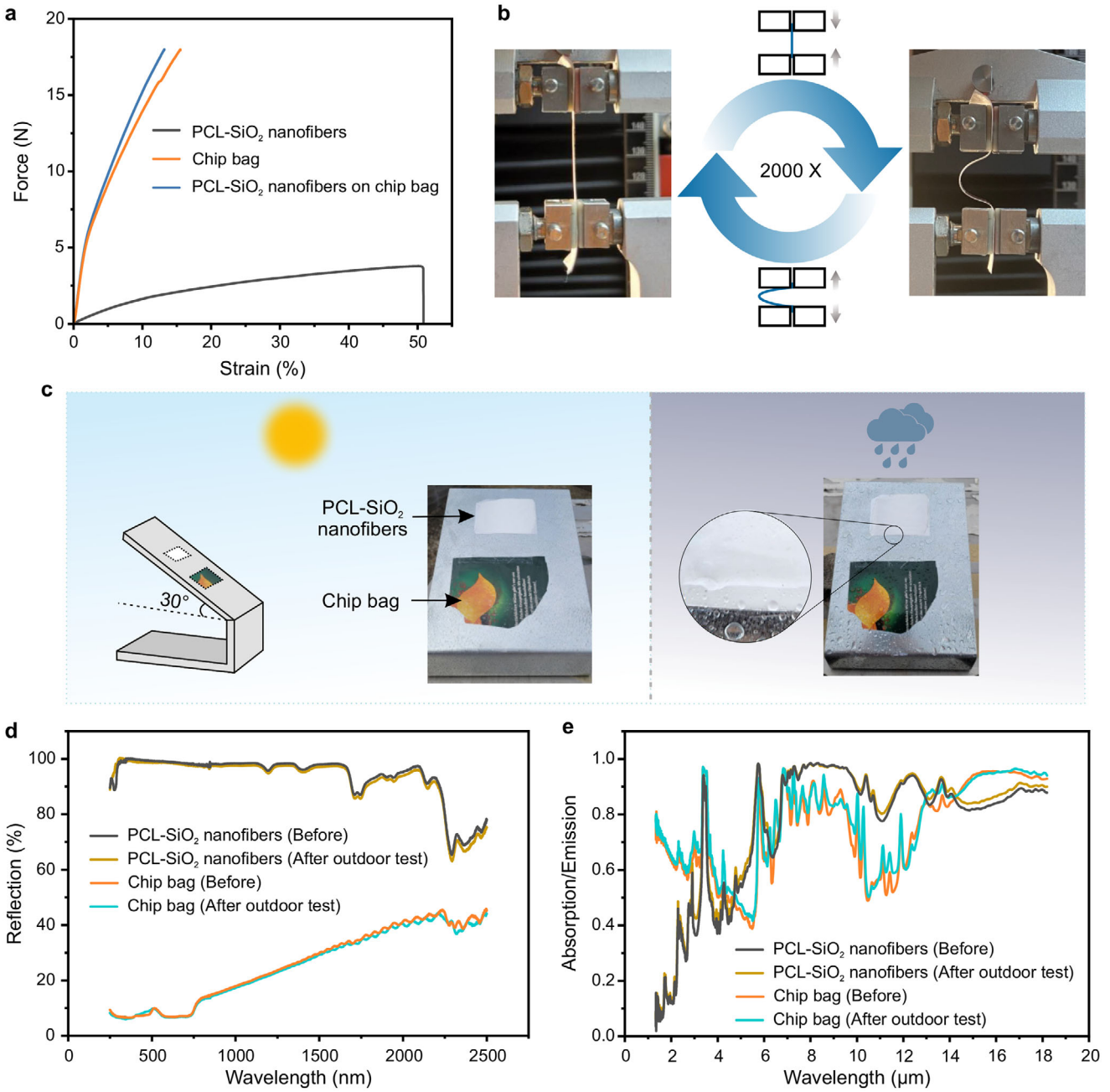

Figure 6. a) Mechanical properties of dual-mode film, free-standing PCL-SiO_2 nanofiber nonwoven and pristine chip bag. d) Bending test of the dual-mode film. c) Photograph and schematic of the setup for outdoor stability testing, along with a photograph of the dual-mode film exposed to the rain. Optical properties, in UV/Vis (d) and MIR (e) ranges, of the dual-mode film before and after one month of outdoor exposure.

with high ambient temperature (32.9 °C), sub-ambient cooling was observed for both PCL-SiO_2 nanofiber and graphite-Al foil (Figure 7e). The steady-state temperatures were 28.1 and 27.2 °C for the PCL-SiO_2 nanofibers and graphite-Al foil, respectively. In "Summer daytime" under solar irradiation of 750 W m^{-2}, the temperature PCL-SiO_2 nanofibers increased by only 1.8 °C, due to its super high solar reflection (98%). The sub-ambient temperature confirms its outstanding passive cooling performance during the daytime. In contrast, the temperature of graphite-Al foil increased above the "ambient", reaching 36.4 °C.

In general, for the cooling mode of the dual-mode device during summer, high solar reflectivity and mid-infrared (MIR) emissivity are essential to minimize solar absorption and maximize thermal emission to outer space. Conversely, in winter, the heating mode benefits from high solar absorption and low MIR emissivity, allowing more solar energy to be converted into heat during the day while reducing nighttime energy losses due to thermal radiation. In this work, the dual-mode film, made from biodegradable polymers and upcycled plastic waste, achieved a remarkable solar reflectivity of 98% and an MIR emissivity of 91% in cooling

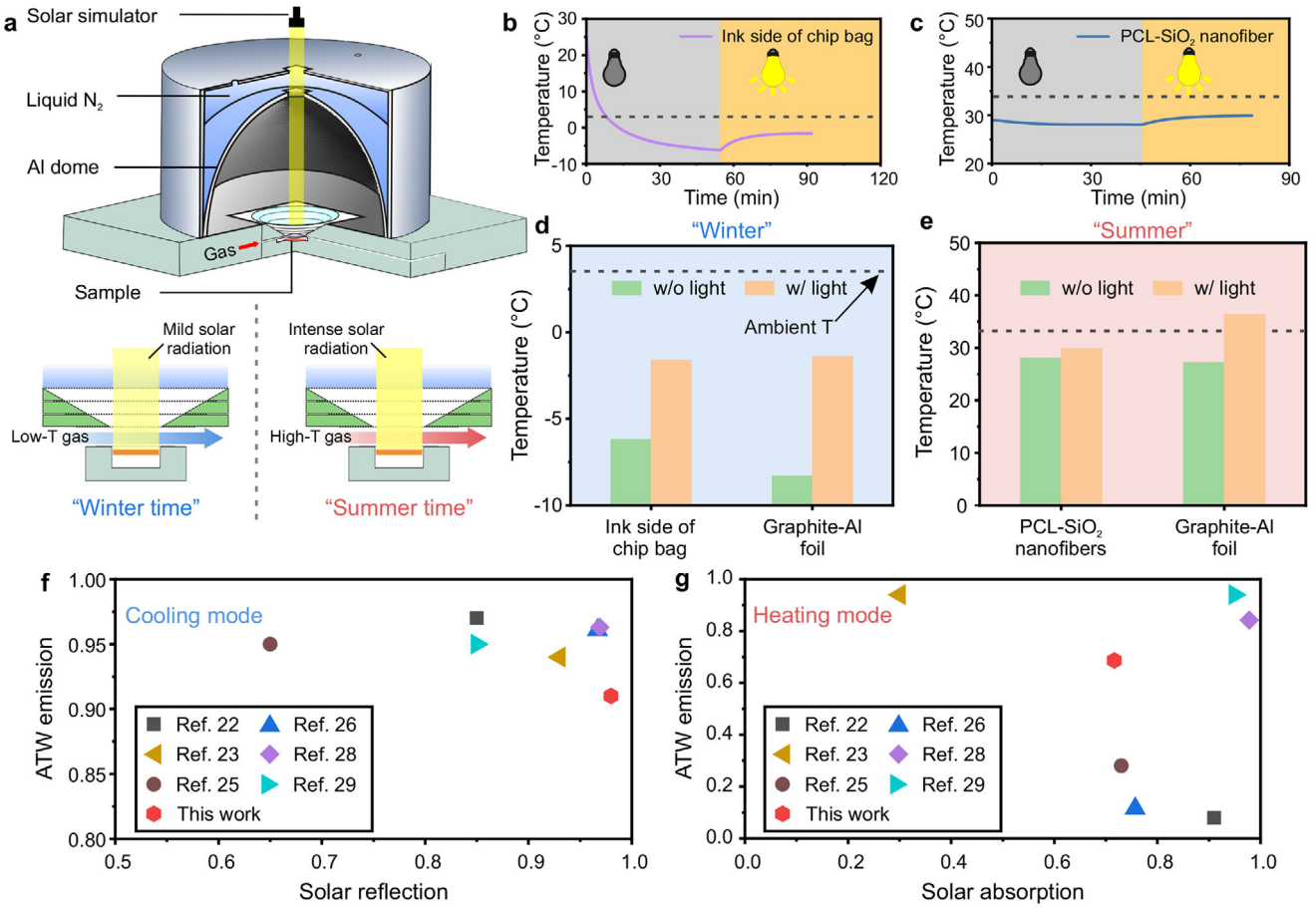

Figure 7. a) Schematic of the indoor setup for characterizing the dual-mode film under "summer" and "winter" conditions. The temperature tracking of the heating side (b), and the cooling side (c), of the dual-mode film. d) The steady-state temperature of the heating side of the dual-mode film (ink side) and graphite-Al foil in "Winter". e) Steady-state temperature of the cooling side of the dual-mode film (PCL-SiO_2 nanofiber) and graphite-Al foil under "Summer" condition. A comparison of the optical properties in both "cooling mode" and "heating mode", between this work and other dual-mode devices reported in literature. Cooling mode: solar reflection and ATW emission (f); Heating mode: solar absorption and ATW emission (g).

mode. In heating mode, it exhibited variable optical properties depending on the pattern of the chip bag waste. For instance, the chip bag shown in Figure 4c demonstrated a solar absorptivity of 71% and an infrared emissivity of 0.69. These values are comparable to, or even surpass, state-of-the-art dual-mode devices (Figure 7f,g), and detailed information on these devices, including optical properties and materials, is listed in Table S1 (Supporting Information). Furthermore, the SBS fabrication process used in this work is highly efficient and suitable for large-scale production, making it possible to retrofit surfaces with passive cooling properties at scale.

3. Conclusion

In summary, a high-performance film with dual-mode functionality for year-round thermal management was developed in this work. By coating highly-scattering PCL-SiO_2 composite nanofibers onto upcycled chip bags waste, the film provides both solar heating and radiative cooling capabilities. During hot conditions, the cooling side of the film, featuring PCL-SiO_2 composite nanofibers, ensures a solar reflection of up to 0.98 and a MIR emissivity of 0.91, resulting in sub-ambient cooling even under intense sunlight. In a cold environment, the significant solar absorption and relatively low MIR emission of the ink side of the chip bag convert sunlight into heat. Consequently, the film maintained a temperature of ≈16.5 °C higher than the open air. Additionally, the easily operable SBS technique facilitates a scalable production of the coating and holds promise for retrofitting such nonwovens also to complex surfaces. The flexible and scalable dual-mode film, derived from sustainable materials, holds the potential to significantly reduce the energy consumption for heating and cooling, thereby making substantial contributions to global warming mitigation.

4. Experimental Section

Materials: Polycaprolactone (Mn = 80000 g mol^{-1}) was purchased from Sigma–Aldrich. Silica nanoparticles (AEROSIL R 202) were obtained from Evonik. Chloroform (>99%) was purchased from VWR.

Fabrication of Nanofibers via Solution Blow Spinning: 5 wt.% PCL solution was prepared by dissolving 0.5 g PCL in 9.5 g chloroform under stirring. For PCL-SiO_2 nanofibers fabrication, 0.05, 0.10, and 0.15 g SiO_2 nanoparticles were added into the PCL solution (10 g, 5 wt.%) to obtain

a m_{SiO2} / m_{PCL} of 0.1, 0.2, and 0.3, followed by stirring until the particles completely dispersed. The resulting solution was then poured into the reservoir of a commercial airbrush (Fengda BD-134, nozzle diameter: 0.3 mm). Subsequently, the solution was sprayed out from the airbrush by compressed air with a pressure of 3 bars. The nanofibers were collected on a rotating collector (rotation speed: 2000 rpm) wrapped with Al foil or chip bag (mirror-like side facing outward). The distance between the collector and the nozzle was ≈20 cm. The obtained nanofiber nonwovens were dried in a fume hood at ambient temperature to remove the residual solvent.

Optical Characterization: Solar reflection measurements were performed using an UV–vis spectrometer (Cary 5000, Agilent Technologies) equipped with an integrating sphere accessory (Labspheres). A Spectralon diffuse reflectance standard (Labspheres) served as the reference. For angular reflectance measurements, the samples were placed inside the integrating sphere and rotated at various angles relative to the incident light beam. Optical properties of samples in the MIR region were determined using FTIR spectroscopy (Vertex 70, Bruker) equipped with a gold-coated integrating sphere accessory (A562, Bruker). A gold mirror was employed as the reference. Absorptance (emittance) was calculated as 1 – Reflectance. Due to the presence of an aluminum layer, transmission was considered negligible.

Tensile and Bending Tests: Tensile and bending tests were performed using a tensile tester (BT1-FR0.5TN.D14, Zwick/Roell, Germany) coupled with a 20 N sensor and a clamping length of 20 mm. Prior to testing, all samples were cut by a hydraulic sample puncher according to DIN 53 504 S3A (Coesfeld Materialtest, Germany). For the tensile test, a testing speed of 5 mm min^{-1} was applied. The cyclic bending test was conducted with an initial strain of 50% (10 mm) and a final strain of 100% (20 mm) at a speed of 1 mm min^{-1}, completing 2000 cycles in total. The thickness of the PCL-SiO_2 nanofiber nonwoven was ≈100 µm.

SEM Measurements: SEM measurements were conducted with a Zeiss Ultra plus (Carl Zeiss AG, Germany). An operating voltage of 3 or 2 kV was applied to obtain the SEM images from the secondary electron detector (in-lens) and backscattered electron detector, respectively.

Contact Angle Measurements: The static contact angles were determined by the sessile drop technique (Dataphysics OCA-20, Filderstadt, Germany) at ambient conditions. 2 µL of Milli-Q water was dropped onto the PCL-SiO_2 nanofiber nonwovens for each measurement. For each sample, three measurements were conducted, and the values are reported as the mean ± σ.

Rooftop Measurements for Heating and Cooling Performance Characterization: Rooftop measurements were carried out on the roof of a four-floor building (May 13–14th, 2024, University of Bayreuth, Bayreuth, Germany) under a clear sky. All the test samples were cut to a size of 5 cm in diameter and embedded inside a Styrofoam to block the conductive heat loss. The temperatures of the samples were determined by a thermocouple (T type) and recorded with a digital multimeter (DAQ6510, Tektronix, Germany) every 5 s. During the measurements, the open-air temperature was recorded next to the samples in the shade. The solar irradiance data were collected from the weather station at the University Bayreuth (Ecological-Botanical Garden, 400 m away from the rooftop measurement).

Finite-Difference Time-Domain (FDTD) Simulation: The scattering efficiency of the PCL nanofibers was performed using 3D FDTD simulation (ANSYS Lumerical, 2020 R2.4). During the simulations, a total-field scatter-field (TFSF) wave source was applied, and the FDTD domain was set to accommodate the PCL nanofibers with various diameters, from 0.1 to 1.5 µm. The entire solar range, 0.2–2.5 µm, was covered in the simulation. A refractive index of 1.46 and 1 was used for the PCL nanofiber and the background, respectively.

Indoor Measurement for Cooling and Heating Performance Characterization: During the measurements, the Al dome was cooled to about −190 °C using liquid nitrogen. The temperature of the dome was maintained constant throughout the measurement by replenishing the liquid nitrogen. Dry air was flushed between the convection shield and measurement cell to regulate the "ambient" temperature. For the "Summer" condition, dried air, preheated to 75 °C using a water bath, was introduced at a volumetric flow rate of 80 ln min^{-1}, resulting in an "ambient" temperature of ≈32.9 °C. For the "Winter" condition, the water bath was set to 30 °C and air was introduced at a flow rate of 35 ln min^{-1}, providing in a "ambient" temperature of ≈3.2 °C. A type T thermocouple was used to monitor the temperature, with data recorded every 5 s using a digital multimeter (DAQ6510, Tektronix, Germany). A solar simulator (AX-LAN400, ScienceTech, Canada) with an illumination area of 5 × 5cm^2 provided AM 1.5 solar light during the daytime measurement. Solar intensity of 100% (≈1000 W m^{-2}) and 70% of one sun were applied for "Summer" and "Winter" conditions, respectively.

Supporting Information

Supporting Information is available from the Wiley Online Library or from the author.

Acknowledgements

The authors gratefully thank Prof. Christoph Thomas for kindly providing the solar radiance data. The authors thank Martina Heider and the Keylab Electron Microscopy (University Bayreuth) for SEM and EDX measurements. The authors acknowledge financial support from the European Research Council (ERC) under the European Union's Horizon 2020 research and innovation program (grant agreement no. 101082087) and from the German Research Foundation within the IRTG Optexc (grant no. 464648186).

Open access funding enabled and organized by Projekt DEAL.

Conflict of Interest

The authors declare no conflict of interest.

Data Availability Statement

The data that support the findings of this study are available from the corresponding author upon reasonable request.

Keywords

biodegradable polymer, passive daytime cooling, radiative cooling, solar heating, solution blow spinning

Received: December 23, 2024
Revised: March 14, 2025
Published online:

[1] *IEA IEA Paris*, https://www.iea.org/reports/world-energy-outlook-2023 (accessed: May 2024).
[2] B. J. v. Ruijven, E. De Cian, I. S. Wing, *Nat. Commun.* **2019**, *10*, 2762.
[3] Y. Li, W. Wang, Y. Wang, Y. Xin, T. He, G. Zhao, *Int. J. Environ. Res. Public Health* **2020**, *18*, 40.
[4] M. A. D. Larsen, S. Petrović, A. M. Radoszynski, R. McKenna, O. Balyk, *Energy Build.* **2020**, *226*, 110397.
[5] V. Ciancio, F. Salata, S. Falasca, G. Curci, I. Golasi, P. de Wilde, *Sustainable Cities Soc* **2020**, *60*, 102213.
[6] T. Huo, R. Cao, H. Du, J. Zhang, W. Cai, B. Liu, *Sci. Total Environ.* **2021**, *772*, 145058.
[7] X. Sun, Y. Sun, Z. Zhou, M. A. Alam, P. Bermel, *Nanophotonics* **2017**, *6*, 997.

[8] D. Zhao, A. Aili, Y. Zhai, S. Xu, G. Tan, X. Yin, R. Yang, *Appl. Phys. Rev.* **2019**, *6*, 021306.
[9] X. Yu, J. Chan, C. Chen, *Nano Energy* **2021**, *88*, 106259.
[10] S. Zeng, S. Pian, M. Su, Z. Wang, M. Wu, X. Liu, M. Chen, Y. Xiang, J. Wu, M. Zhang, Q. Cen, Y. Tang, X. Zhou, Z. Huang, R. Wang, A. Tunuhe, X. Sun, Z. Xia, M. Tian, M. Chen, X. Ma, L. Yang, J. Zhou, H. Zhou, Q. Yang, X. Li, Y. Ma, G. Tao, *Science* **2021**, *373*, 692.
[11] R. Yang, F. Xie, Y. Li, X. Wang, Y. Pan, C. Liu, C. Shen, X. Liu, *Adv. Nanocompos.* **2024**, *1*, 86.
[12] A. P. Raman, M. A. Anoma, L. Zhu, E. Rephaeli, S. Fan, *Nature* **2014**, *515*, 540.
[13] T. Li, Y. Zhai, S. He, W. Gan, Z. Wei, M. Heidarinejad, D. Dalgo, R. Mi, X. Zhao, J. Song, J. Dai, C. Chen, A. Aili, A. Vellore, A. Martini, R. Yang, J. Srebric, X. Yin, L. Hu, *Science* **2019**, *364*, 760.
[14] J. Mandal, Y. Fu, A. C. Overvig, M. Jia, K. Sun, N. N. Shi, H. Zhou, X. Xiao, N. Yu, Y. Yang, *Science* **2018**, *362*, 315.
[15] X. Zhao, T. Li, H. Xie, H. Liu, L. Wang, Y. Qu, S. C. Li, S. Liu, A. H. Brozena, Z. Yu, J. Srebric, L. Hu, *Science* **2023**, *382*, 684.
[16] K. Lin, S. Chen, Y. Zeng, T. C. Ho, Y. Zhu, X. Wang, F. Liu, B. Huang, C. Y. Chao, Z. Wang, C. Y. Tso, *Science* **2023**, *382*, 691.
[17] J. Song, W. Zhang, Z. Sun, M. Pan, F. Tian, X. Li, M. Ye, X. Deng, *Nat. Commun.* **2022**, *13*, 4805.
[18] S. Zhou, P. Chen, C. Xiao, Y. Ge, H. Gao, *RSC Adv.* **2023**, *13*, 31738.
[19] Y. An, Y. Fu, J.-G. Dai, X. Yin, D. Lei, *Cell Rep. Phys. Sci.* **2022**, *3*, 101098.
[20] J. Wang, G. Tan, R. Yang, D. Zhao, *Cell Rep. Phys. Sci.* **2022**, *3*, 101198.
[21] M. Liao, D. Banerjee, T. Hallberg, C. Akerlind, M. M. Alam, Q. Zhang, H. Kariis, D. Zhao, M. P. Jonsson, *Adv. Sci.* **2023**, *10*, 2206510.
[22] Q. Zhang, Y. Lv, Y. Wang, S. Yu, C. Li, R. Ma, Y. Chen, *Nat. Commun.* **2022**, *13*, 4874.
[23] Y. Dong, W. Meng, F. Wang, H. Han, H. Liang, X. Li, Y. Zou, C. Yang, Z. Xu, Y. Yan, Z. Cheng, *Nano Lett.* **2023**, *23*, 9034.
[24] K. Tang, K. Dong, J. Li, M. P. Gordon, F. G. Reichertz, H. Kim, Y. Rho, Q. Wang, C. Y. Lin, C. P. Grigoropoulos, A. Javey, J. J. Urban, J. Yao, R. Levinson, J. Wu, *Science* **2021**, *374*, 1504.
[25] Q. Zhang, Y. Wang, Y. Lv, S. Yu, R. Ma, *Proc. Natl. Acad. Sci. U. S. A.* **2022**, *119*, 2207353119.
[26] M. Shi, Z. Song, J. Ni, X. Du, Y. Cao, Y. Yang, W. Wang, J. Wang, *ACS Nano* **2023**, *17*, 2029.
[27] P. Yang, J. He, Y. Ju, Q. Zhang, Y. Wu, Z. Xia, L. Chen, S. Tang, *Adv. Sci.* **2023**, *10*, 2206176.
[28] B. Xiang, R. Zhang, X. Zeng, Y. Luo, Z. Luo, *Adv. Fiber Mater.* **2022**, *4*, 1058.
[29] B. Dai, X. Li, T. Xu, X. Zhang, *ACS Appl. Mater. Interfaces* **2022**, *14*, 18877.
[30] W. B. Han, S. Y. Heo, D. Kim, S. M. Yang, G. J. Ko, G. J. Lee, D. J. Kim, K. Rajaram, J. H. Lee, J. W. Shin, T. M. Jang, S. Han, H. Kang, J. H. Lim, D. H. Kim, S. H. Kim, Y. M. Song, S. W. Hwang, *Sci. Adv.* **2023**, *9*, adf5883.
[31] X. Liu, M. Zhang, Y. Hou, Y. Pan, C. Liu, C. Shen, *Adv. Funct. Mater.* **2022**, *32*, 2207414.
[32] C. Park, C. Park, X. Nie, J. Lee, Y. S. Kim, Y. Yoo, *ACS Sustainable Chem. Eng.* **2022**, *10*, 7091.
[33] S. H. Alkandari, M. Ching, J. C. Lightfoot, N. Berri, H. S. Leese, B. Castro-Dominguez, *ACS Appl. Eng. Mater.* **2024**, *2*, 1515.
[34] Z. Jiang, S. Piao, T. Park, S. Li, Y. Kim, E. Lee, C. Bae, Y. Lee, H. J. Im, J. Oh, Y. Piao, K. Lee, *Adv. Mater. Interfaces* **2024**, *11*, 2301047.
[35] A. O. M. Salehi, S. H. Keshel, F. Sefat, L. Tayebi, *Mater. Today Commun.* **2021**, *27*, 102402.
[36] R. M. Mohamed, K. Yusoh, *Adv. Mater. Res.* **2015**, *1134*, 249.
[37] D. Goldberg, *J. Environ. Polym. Degr.* **1995**, *3*, 61.
[38] M. Bartnikowski, T. R. Dargaville, S. Ivanovski, D. W. Hutmacher, *Prog. Polym. Sci.* **2019**, *96*, 1.
[39] P. Ang, S. R. Mothe, L. R. Chennamaneni, F. Aidil, H. H. Khoo, P. Thoniyot, *ACS Sustainable Chem. Eng.* **2020**, *9*, 669.
[40] J. L. Daristotle, A. M. Behrens, A. D. Sandler, P. Kofinas, *ACS Appl. Mater. Interfaces* **2016**, *8*, 34951.
[41] J. Lv, X. Yin, R. Li, J. Chen, Q. Lin, L. Zhu, *Polym. Eng. Sci.* **2019**, *59*, E171.
[42] Z. Li, Z. Cui, L. Zhao, N. Hussain, Y. Zhao, C. Yang, X. Jiang, L. Li, J. Song, B. Zhang, Z. Cheng, H. Wu, *Sci. Adv.* **2022**, *8*, abn3690.
[43] S. A. H. Ravandi, M. Sadrjahani, A. Valipouri, F. Dabirian, F. K. Ko, *Text. Res. J.* **2022**, *92*, 5130.
[44] *Solar Spectral Irradiance: Air Mass 1.5*, http://rredc.nrel.gov/solar/spectra/am1.5 (accessed: May 2024).
[45] B. Zhu, W. Li, Q. Zhang, D. Li, X. Liu, Y. Wang, N. Xu, Z. Wu, J. Li, X. Li, P. B. Catrysse, W. Xu, S. Fan, J. Zhu, *Nat. Nanotechnol.* **2021**, *16*, 1342.
[46] H. Kim, S. McSherry, B. Brown, A. Lenert, *ACS Appl. Mater. Interfaces* **2020**, *12*, 43553.
[47] G. K. Deshwal, N. R. Panjagari, *J. Food Sci. Technol.* **2020**, *57*, 2377.
[48] A. S. Bauer, M. Tacker, I. Uysal-Unalan, R. M. S. Cruz, T. Varzakas, V. Krauter, *Foods* **2021**, *10*, 2702.
[49] Q. Song, M. Retsch, *ACS Sustainable Chem. Eng.* **2023**, *11*, 10631.
[50] Q. Song, T. Tran, K. Herrmann, H. Schmalz, M. Retsch, *Adv. Mater. Technol.* **2023**, *8*, 2300444.
[51] R. Yaseri, M. Fadaie, E. Mirzaei, H. Samadian, A. Ebrahiminezhad, *Sci. Rep.* **2023**, *13*, 9434.
[52] Q. Song, T. Tran, K. Herrmann, T. Lauster, M. Breitenbach, M. Retsch, *Cell Rep. Phys. Sci.* **2022**, *3*, 100986.